



Research article

An innovative approach for assessing coronary artery lesions: Fusion of wrist pulse and photoplethysmography using a multi-sensor pulse diagnostic device

M.A. Xiaotian^a, Rui Guo^{a,*}, Chunke Zhang^a, Jianjun Yan^{b,**}, Guangyao Zhu^b, Wenjie Wu^a, Haixia Yan^a, Leixin Hong^a

^a School of Traditional Chinese Medicine, Shanghai University of Traditional Chinese Medicine, Shanghai, 201203, China

^b Institute of Intelligent Perception and Diagnosis, School of Mechanical and Power Engineering, East China University of Science and Technology, Shanghai, 200237, China

ARTICLE INFO

Keywords:

Coronary heart disease (CHD)
Wrist pressure pulse waves
Fingertip photoplethysmography (FPPG)
Assessment of coronary artery occlusion severity
Random forest-based model

ABSTRACT

Coronary heart disease (CHD) is a leading cause of mortality globally and poses a significant threat to public health. Coronary angiography (CAG) is a gold standard for the clinical diagnosis of CHD, but its invasiveness restricts its widespread application. In this study, we utilized a pulse diagnostic device equipped with pressure and photoelectric sensors to synchronously and non-invasively capture wrist pressure pulse waves and fingertip photoplethysmography (FPPG) of patients undergoing CAG. The extracted features were utilized in constructing random forest-based models to assessing the severity of coronary artery lesions. Notably, Model 3, incorporating both wrist pulse and FPPG features, surpassed Model 1 (solely utilizing wrist pulse features) and Model 2 (solely utilizing FPPG features). Model3 achieved an Accuracy, Precision, Recall, and F1-score of 78.79%, 78.69%, 78.79%, and 78.70%, respectively. Compared to Model1 and Model2, Model 3 exhibited improvements by 4.55%, 5.25%, 4.55%, and 5.12%, and 6.06%, 6.58%, 6.06%, and 6.54% respectively. This fusion of wrist pulse and FPPG features in Model 3 highlights the advantages of multi-source information fusion for model optimization. Additionally, this research provides invaluable insights into the novel development of diagnostic devices imbued with TCM principles and their potential in managing cardiovascular diseases.

1. Introduction

Coronary heart disease (CHD), marked by the occlusion and stenosis of coronary arteries, which leads to myocardial ischemia and related heart conditions, remains a primary cause of global mortality [1]. Its prevalence is concerning, affecting approximately 20.1 million Americans aged 20 or older according to the NHANES data from 2015 to 2018, indicating an overall prevalence of 7.2% among U.S. adults [2]. Similarly, the mortality rate of CHD among Chinese residents has rising since 2012, reaching 130.14 per 100,000 in 2019, as reported by the China Health Statistical Yearbook 2020 [3]. The rising prevalence of CHD presents a significant public health

* Corresponding author.

** Corresponding author. School of Mechanical and Power Engineering, East China University of Science and Technology, Shanghai 200237, China.

E-mail addresses: guoruier@sina.com (R. Guo), jjyan@ecust.edu.cn (J. Yan).

<https://doi.org/10.1016/j.heliyon.2024.e28652>

Received 25 August 2023; Received in revised form 20 March 2024; Accepted 21 March 2024

Available online 27 March 2024

2405-8440/© 2024 The Authors. Published by Elsevier Ltd. This is an open access article under the CC BY-NC license (<http://creativecommons.org/licenses/by-nc/4.0/>).

challenge worldwide, resulting in substantial economic and healthcare burdens. Consequently, the urgency for accurate diagnosis and effective prevention strategies cannot be overstated.

Abnormal changes in coronary artery function and structure have been identified as the primary causes of clinical cardiovascular risk events in previous studies [4–6], emphasizing the importance of identifying coronary artery lesions. However, coronary angiography (CAG) [7], considered the gold standard for diagnosing CHD, has limitations due to its invasive nature, risk of allergic reactions, and potential complications, making it unsuitable for early screening of patients with suspected CHD and mild symptoms. Similarly, while other clinical examinations such as intravascular ultrasound (IVUS) [8] and coronary computed tomography angiography (CCTA) [9] are available for diagnosing coronary lesions, their high cost, operational complexity or invasiveness hinder their broad application in disease surveillance and prevention.

Pulse diagnosis is a unique diagnostic method in traditional Chinese medicine, wherein doctors can gather pathological information from patients by feeling the pulsations at the radial artery using their fingers, aiding in diagnosis. In fact, this pulse-taking method, based on the rhythmic contractions of the heart, conveys critical information about the cardiovascular system [10,11]. The arterial pulse wave embodies pulsatile fluctuations of blood vessel pressure, velocity, and diameter. Alterations in these pulse wave characteristics can indicate a spectrum of cardiovascular diseases, including arterial stiffness, hypertension, atherosclerosis, and other anomalies. Furthermore, during circulation, blood traverses through peripheral micro-arteries, capillaries, and micro-venules, leading to pulsatile changes in blood volume within these microvessels due to cardiac pulsations. This volume pulse wave, measured at the fingertip using photoplethysmography, reflects essential cardiovascular data, such as cardiac function, blood flow, peripheral vessels, and microcirculation. This information is vital for the diagnosis, monitoring, and management of cardiovascular diseases.

Research has demonstrated the feasibility of identifying and diagnosing diseases using wrist pressure pulse wave and PPG (photoplethysmography) blood volume pulse wave signals, which offers advantages such as convenience, effectiveness, and non-invasiveness. For example, Amjed S. Al Fahoum et al. [12] achieved an accuracy rate of 89.37% in identifying 160 patients with five different cardiovascular diseases using PPG signals and feature selection-based classifiers. Technological advancements have catalyzed development of pulse diagnostic devices incorporating multiple sensors [13]. In a study by Jianjun YAN et al. [14], a multi-sensor pulse diagnostic device (as shown in Fig. 1) were employed to capture wrist pressure pulse wave and fingertip photoplethysmography (FPPG) signals. From these, 82-dimensional features were extracted and a blood pressure assessment model was developed using the gradient boosting decision tree regression algorithm. The evaluation results adhered to performance standards of the Association for the Advancement of Medical Instrumentation and British Hypertension Society. These findings emphasized the potential advantages of non-invasive and convenient diagnostic methods, showcasing the benefits of pulse diagnostic devices with multiple sensors. These devices capture multi-channel physiological signals simultaneously, facilitating comprehensive pathophysiological information collection, thereby enhancing health assessments and disease identification accuracy.

This study introduced a novel method to assess the severity of coronary artery obstruction in CHD patients and those suspected CHD using a non-invasive technology. The proposed approach utilize a pulse diagnostic device equipped with pressure and photoelectric sensors to synchronously collect wrist pressure pulse waves and FPPG of patients undergoing CAG. Features extracted from these signals are employed in constructing random forest-based models to assess the severity of coronary artery lesions. Additionally, this study explored the potential value of wearable pulse diagnostic devices that integrated multi-source information fusion technology for comprehensive and real-time out-of-hospital health monitoring. This capability facilitates, early detection, prediction and warning. Utilizing wearable devices with multi-source information fusion technology presented a promising pathway for personalized healthcare and proactive disease management.



Fig. 1. The wearable hardware component of ZY-I type pulse diagnostic device.

2. Data and methods

2.1. Participants

In this study, a total of 133 participants were recruited from the Yueyang Hospital of Integrated Traditional Chinese and Western Medicine, and Shuguang Hospital, both are affiliated with Shanghai University of Traditional Chinese Medicine, between December 2020 and July 2021.

Participants were considered for inclusion if they (1) presented clinically with CHD and were scheduled for coronary angiography, (2) were aged 40 or above, and (3) provided written informed consent.

Participants were excluded if they (1) experienced chest pain resulting from heart diseases other than CHD, severe neurosis, menopausal syndrome, or cervical spondylosis, (2) had significant primary diseases of the liver, kidney, or hematopoietic system, (3) suffered from psychiatric disorders, (4) had a history of coronary artery intervention or bypass surgery, (5) were unable to complete pulse data collection, or (6) had incomplete medical records.

Diagnostic criteria for CHD were based on the guidelines provided by the American College of Cardiology/American Heart Association (ACC/AHA) (2007) [15]. The confirmation of CHD required the presence of coronary angiography, which identified stenosis of at least one coronary vessel, including the left main branch, left anterior descending branch (including diagonal branch), left circumflex branch (including obtuse marginal branch), and right coronary artery (including posterior descending branch and left posterior ventricular branch), with a severity of $\geq 50\%$ at the most severe point.

Ethical approval for this study was obtained from Ethics Committee of the Shanghai University of Traditional Chinese Medicine. All participants voluntarily agreed to take part in the study and provided informed consent. The confidentiality of personal information was strictly maintained.

2.2. Grouping

The patients were categorized into three groups based on the severity of stenosis in the primary coronary vessel with the most severe coronary artery stenosis.

Group 1 :Stenosis in the primary coronary vessel $< 50\%$

Group 2 :Stenosis in the primary coronary vessel ranging from 50% to $< 70\%$

Group 3 :Stenosis in the primary coronary vessel $\geq 70\%$.

2.3. Participant data

2.3.1. Participant demographics

Participant demographics were collected, including information on their sex, age, blood pressure, height and weight. Height and weight measurements were taken in an upright position with shoes off using a Height and Weight Measurement Instrument. To determine each participant's body mass index (BMI), the following formula was applied: $BMI = \text{weight (kg)}/[\text{height (m)}]^2$.

2.3.2. Acquisition of wrist pulse and FPPG signals

The ZY-I type pulse diagnostic device, featuring multiple sensors including pressure and photoelectric sensors, was developed jointly by the Shanghai University of Traditional Chinese Medicine and the East China University of Science and Technology. This advanced device was used for the acquisition and analysis of wrist pulse and FPPG signals, providing valuable insights into

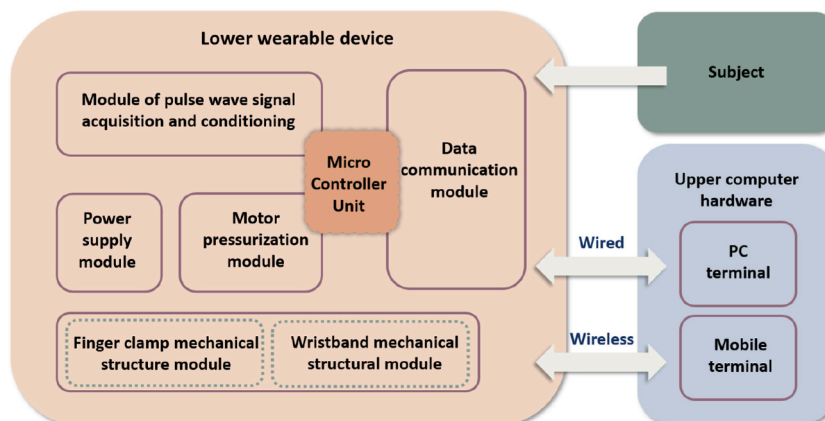


Fig. 2. Overall structure of the wearable hardware system.

cardiovascular health. The wearable hardware component of ZY-I type device is illustrated in Fig. 1.

The wristband hardware system of pulse diagnosis device with multiple sensors, is depicted in Fig. 2. It comprises two primary components: the upper computer (Host) and the lower wearable device (Slave). The upper computer, which includes devices such as computers and smartphones, is equipped with a pulse waveform acquisition and analysis program. It enables functions such as instruction control, data reception and storage, as well as signal processing and analysis for the wearable pulse diagnosis wristband. The lower wearable device serves as the pulse diagnosis wristband itself, responsible for signal acquisition, data communication, pressure application, and comfortable wearing.

Prior to signals acquisition, participants were instructed to sit in a quiet environment for a minimum of 3 min, maintaining calm breathing and relaxation. They were instructed to extend their forearms and palms facing up.

The wrist pulse acquisition terminal of the ZY-I-type pulse diagnostic device was securely positioned at the styloid process of left radius. Additionally, the fingertip photoelectric splint was firmly attached to the tip of the middle finger on the left hand (Fig. 3). The wrist pulse and FPPG signals were recorded for 60 s at a sample rate of 4000 Hz when the wrist pulse signal reached its peak amplitude and remained stable.

2.4. Processing of wrist pulse and FPPG signals

The flowchart illustrating the processing of wrist pulse and FPPG signals is presented in Fig. 4. Initially, the concurrently collected original pulse wave signals undergo preprocessing, which includes filtering, baseline drift removal, and the extraction of single-cycles. Following this, during the feature engineering stage, time-domain features of wrist pressure pulse wave and FPPG signals, along with Pulse Wave Transit Time (PWTT), are extracted to form the feature set for model prediction. Subsequently, these features are employed to establish a prediction model based on the random forest algorithm. The detailed process is outlined as follows.

2.4.1. Signals preprocessing

In process of collection data from wearable hardware of pulse diagnostic device, the sensors are susceptible to various external environmental factors, such as patient limb tremors, breathing, instrument mechanical vibrations, and power frequency interference. These factors result in a varying degree of baseline drift and high/low-frequency noise in the output signals. Additionally, the raw pulse wave signals obtained contain multiple cycles, necessitating the extraction of individual cycles for detailed analysis. Hence, preprocessing is essential before analyzing the pulse wave signals, primarily involving filtering, baseline drift removal, and single-cycle extraction.

2.4.1.1. Signal filtering. To achieve zero-phase filtering while preserving the temporal characteristics of the signal, we adopt a combination of bidirectional filtering and Butterworth digital filtering. This approach effectively removes frequency components within the range of 0.5–20Hz.

2.4.1.2. Removing baseline drift. The filtered pulse wave signal exhibits a noticeable fluctuating trend, as shown in Fig. 5. To remove baseline drift, we employed a method involving the fitting of cubic spline curves. The process begins by locating the trough points of each cycle. These points are then used to fit the baseline. Finally, the overall signal fluctuation is corrected by calculating the difference between the signal and the baseline.

Due to the prominence of the main wave peak, we first located the peak points. Subsequently, we identified the trough points by searching for the points of minimum values. A window segmentation method was introduced for the positioning of peak points, detailed as follows.

- (1) Divide the filtered pulse wave into n segments with a window length W for each waveform.

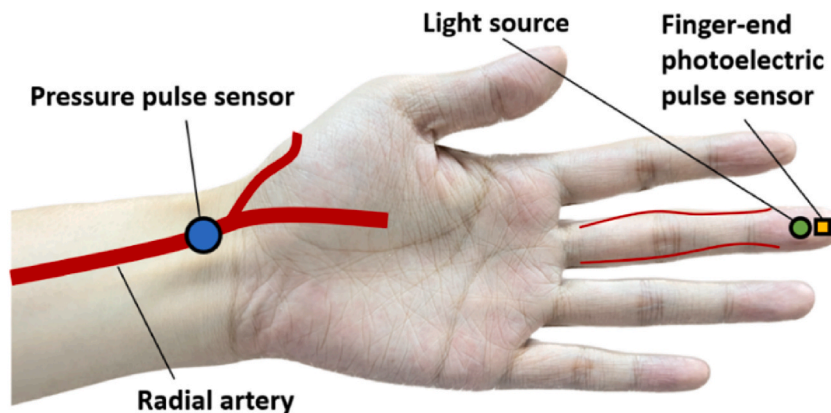


Fig. 3. Distribution scheme for pulse sensors.

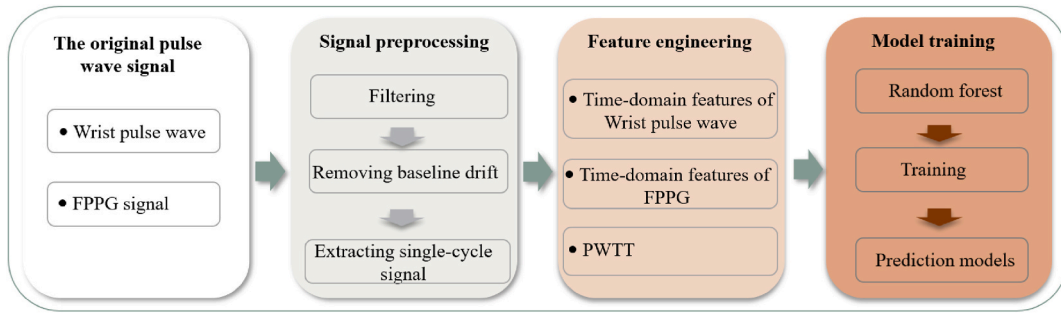


Fig. 4. Flowchart of data processing.

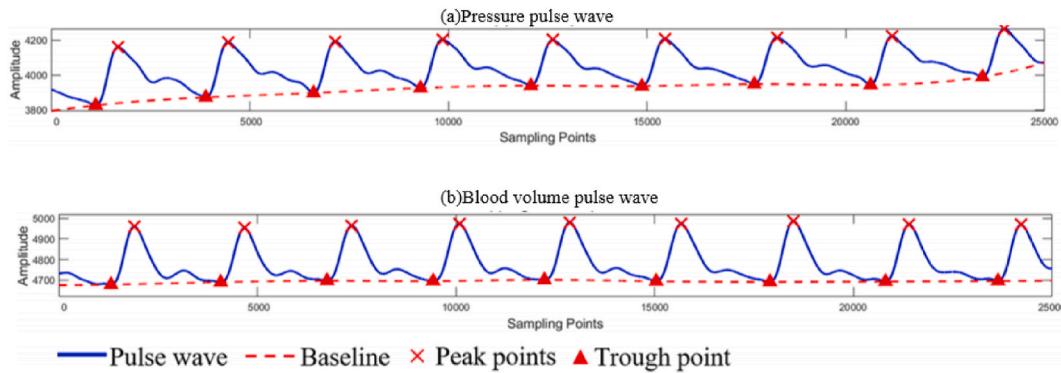


Fig. 5. Filtered pulse wave signals: wrist pressure pulse wave, FPPG pulse wave.

- (2) Identify the maximum point in each segment window waveform and record its position.
- (3) Starting from the first window, compare the maximum value within the window with the maximum values in the adjacent left and right 10 windows. If the point is the maximum value, mark it as a peak point. Then, slide to the next window and repeat this process until the last window.

In this process, W is set based on the sampling frequency (f_s), where $W = f_s/32$. The total number of segments (n) is the total length of the pulse wave divided by W . Considering that the sampling frequency of the pulse diagnostic device is 4000Hz, and a single cycle of the pulse wave has approximately 2000–3000 sampling points, W is set to 150. Compared to the traditional window sliding algorithm, which moves one sampling point at a time, the window segmentation method designed in this study offers a faster processing speed for high-sampling-frequency pulse wave signals. As illustrated in Fig. 5, precise positioning of the peak points has been achieved for different pulse waves. Fig. 6 demonstrates the fitting of a cubic spline curve through the marked trough points and the effect of removing the baseline, showing that each pulse wave cycle has been aligned to the same horizontal line.

2.4.1.3. *Single-cycle signal extraction.* The pulse wave signal is a quasi-periodic signal. Due to the potential influence of external factors, each single-cycle signal may exhibit subtle waveform differences. To preserve the representative characteristics of these

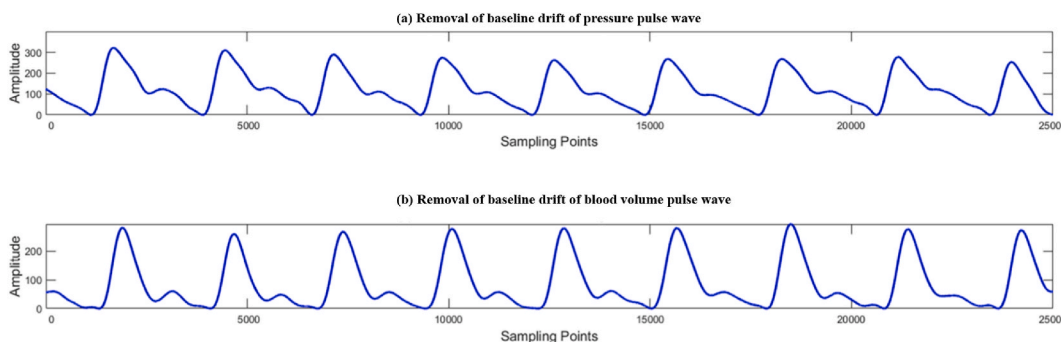


Fig. 6. The effect of baseline drift removal.

signals, it is necessary to average all extracted cycles. The specific extraction process is as follows.

- (1) Segment multiple single-cycle waveforms based on the pulse wave trough point identified in the previous section, as illustrated in Fig. 7(a).
- (2) Exclude abnormal single-cycle waveforms potentially caused by body movements. This is mainly applicable in cases where the waveform length is excessively long or short, or the amplitude is too large.
- (3) Calculate the maximum length of each single-cycle waveform and apply zero-padding to values below this length.
- (4) Compute the average value of all cycles at each sampling point. Subsequently, remove the excess zero-mean sampling points at the end, resulting in the single-cycle waveform depicted in Fig. 7(b).

2.4.2. Features extraction of wrist pulse and FPPG signals

2.4.2.1. A representative cycle of pulse waveform and its characteristic points. The Time-Domain Analysis Method (TDM) primarily focuses on analyzing the waveform of a representative cycle of a pulse signal [16]. It involves defining characteristic points with physiological and pathological significance and extracting corresponding feature parameters. In this study, we primarily employed the feature point locating method [17] to accurately identify seven feature points within a cardiac cycle of the pulse waveform. These are marked as A-G in Fig. 8 and their physiological significance is detailed in Table 1.

2.4.2.2. Extraction methods of time-domain features of a cycle of pulse waveform. Pulse diagnostic instruments commonly output three types of pulse waveforms: Type I (with one peak) as shown in Fig. 9(a), Type II (with two peaks) as depicted in Fig. 9(b), and Type III (with three peaks), illustrated in Fig. 9(c).

The flowchart illustrating the seven feature points for these three types of pulse waveforms is presented in Fig. 10. To locate the three peaks and two troughs in the waveform, digital signal processing methods such as plane geometry and differential diagrams are utilized. For a Type I waveform (with one peak), points D and E are extracted to convert it to the Type II pulse waveform. Similarly, for a Type II waveform (with two peaks), points B and C are extracted to convert it to a Type III pulse waveform.

For a Type III pulse waveform, see Fig. 11(a), which distinctly exhibits three peaks and two troughs, the extraction of the seven feature points proceeds as follows.

- (1) Obtain the first-order differential signal of the pulse signal, as shown in Fig. 11(b) and the second-order differential signal of the pulse signal, as illustrated in Fig. 11(c).
- (2) Identify the set of zero points in the first-order differential signal. The horizontal coordinate of each point in this set corresponds to the horizontal coordinate of an extremum point of the pulse waveform. Determine whether each point is a local minimum or maximum based on the positive or negative value of the corresponding horizontal coordinate in the second-order differential signal.
- (3) Determine points B, C, D, E, and F based on the relative order of the horizontal coordinates of the points in the set and finally compute the time-domain features.

2.4.2.3. Extracted time-domain feature of wrist pulse and FPPG signals. The amplitudes and phases of these identified peaks and troughs provide essential information about physiological and pathological conditions [18]. By precisely these seven features points in Fig. 8 we can effectively describe the temporal variations of the waveform.

Based on the amplitudes and phases of these seven features points, we extracted 21 time-domain features, including 7 amplitude features, 5 time features, and 9 proportion features from wrist pressure pulse wave, shown in Table 2. Similarly, the same processing was applied to extract time-domain features from FPPG signals, including following features such as h1_ppg, h2_ppg, h3_ppg, h4_ppg, h5_ppg, h2/h1_ppg, h3/h1_ppg, h4/h1_ppg, h5/h1_ppg, t1_ppg, t2_ppg, t3_ppg, t4_ppg, t5_ppg, T_ppg, t1/T_ppg, t4/T_ppg, t1/t4_ppg, t5/t4_ppg, w1_ppg, w2_ppg, w1/T_ppg, w2/T_ppg.

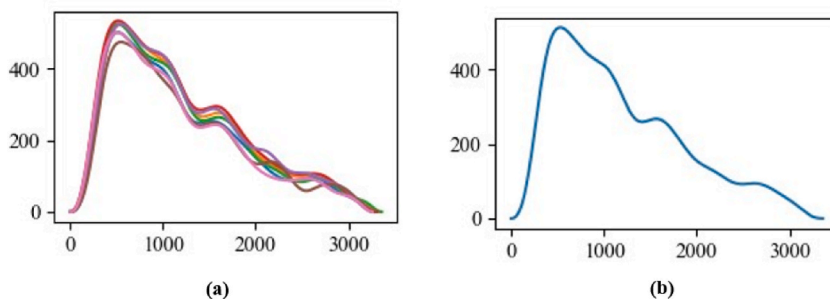


Fig. 7. (a) Multiple single-cycle waveforms in the original pulse wave signal. (b) Average waveform of the single-cycle pulse wave.

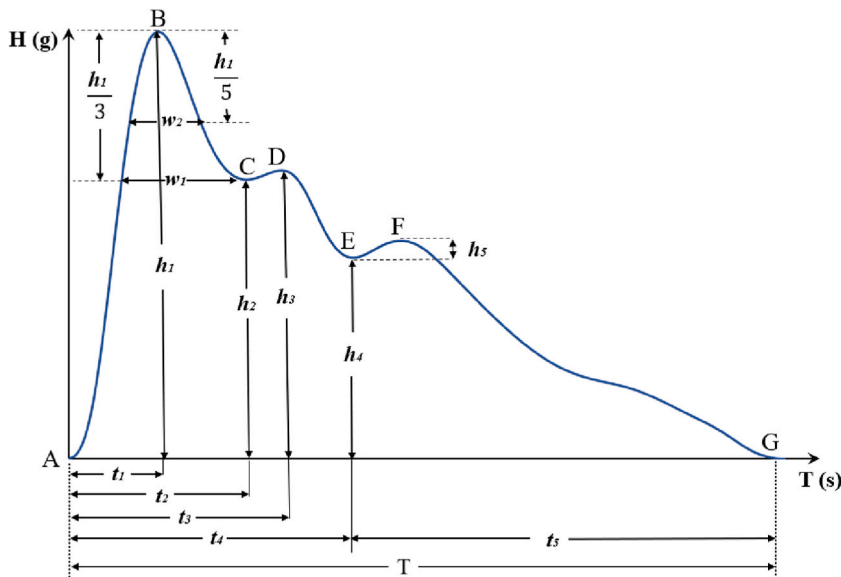


Fig. 8. One cardiac cycle of pulse waveform with X-axis and Y -axis representing time and amplitude, respectively.

Table 1
Physiological significance of pulse signal reference points.

Reference point	Meaning
A	Start point
B	Main wave crest
C	Main wave gap
D	Tidal wave peak
E	Dicrotic notch
F	Dicrotic wave peak
G	End point

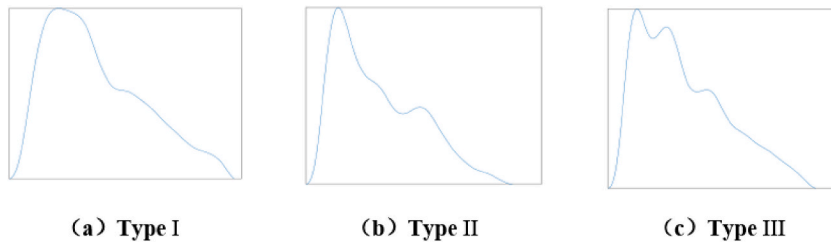


Fig. 9. Pulse waveforms with different peaks.

2.4.2.4. *Calculating PWTT.* Pulse Wave Transit Time (PWTT) is a physiological parameter indicating the duration required for a pulse wave to traverse the distance between two arterial sites within the human body. The calculation involves measuring the time delay between the pulse wave’s initiation at one arterial site to its arrival at another. In the context of this investigation, “PWTT” refers to the pulse wave transit time from the radial artery at the wrist to the vessels located at the fingertip.

The step-by-step calculation process for PWTT is outlined as follows.

- (1) Record the position of peak point of each cycle of the wrist pulse and FPPG signals.
- (2) Determine the number of sample points ‘n’ between the peak points of the two types of signals in the same cycle. Calculate the time difference ‘t’ based on the sampling frequency ‘fs’ by applying the formula $t = n/fs$.
- (3) Compute the average time difference for each cycle between the two types of signals, ultimately obtaining the PWTT value.

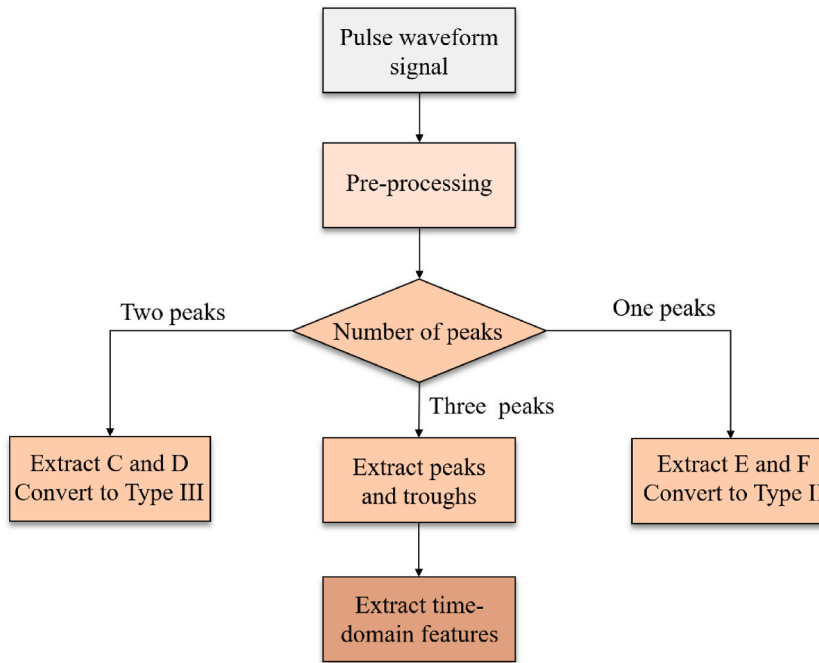


Fig. 10. Flow chart of feature point positioning.

2.5. Statistical analysis

Statistical analysis was performed using SPSS 25.0 (IBM, Armonk, NY, USA) to compare the clinical data, wrist pulse features and FPPG features among different groups of patients. The Wilcoxon-Mann-Whitney nonparametric test was employed to compare continuous variables, with the results presented as median values and quartile ([M (Q1, Q3)]). Categorical variables were compared using the chi-squared test, and the results were expressed as percentages. All reported P values were two-tailed, and those less than 0.05 were considered statistically significant.

2.6. Modeling method

The random forest (RF) algorithm is a widely used ensemble method for classification and regression in biomedical applications. It is an improvement over the decision tree algorithm, as it constructs multiple decision trees (or regression functions) and combines their predictions to get the final result [19]. Each decision tree is established independently on a randomly extracted sample subset of the data, and all the trees in the random forest are uniformly distributed. While an individual tree may have limited classification capability, the random forest makes predictions by aggregating the results of a large number of randomly generated decisions and performing statistical analysis on their classification outcomes. The process of RF classification process is showed in Fig. 12.

In this study, machine learning (ML) was performed by MATLAB 2015(Math Works Co.) and the RF algorithm was employed to develop a model for assessing the severity of coronary occlusion. A 5-fold cross validation was performed on dataset, which 80% of data randomly assigned as the training set and the remaining 20% as the test set. The models were retested five times, and the mean value was calculated for prediction.

The confusion matrix is a visual tool used to assess a model's performance by comparing its predicted values with actual measurements. Table 3 illustrates the confusion matrix, where the Actual Positive row represents the instances that are truly positive in the dataset. The Actual Negative row represents the instances that are truly negative. The Predicted Positive column represents the instances predicted as positive by the model and the Predicted Negative column represents the instances predicted as negative. To evaluate the model's performance, we calculated Accuracy, Precision, Recall, and F1-score using formulas (1)-(4).

Accuracy is a fundamental metric that provides a comprehensive assessment of the model's correctness, quantifying the proportion of correctly classified instances relative to the total number of instances. We calculated accuracy using formula (1):

$$\text{Accuracy} = \frac{\text{TP} + \text{TN}}{\text{TP} + \text{FN} + \text{FP} + \text{TN}} \quad (1)$$

Precision is a crucial metric that evaluates the model's ability to accurately identify positive instances, measuring the proportion of correctly predicted positive instances relative to all instances predicted as positive. Precision was computed using formula (2):

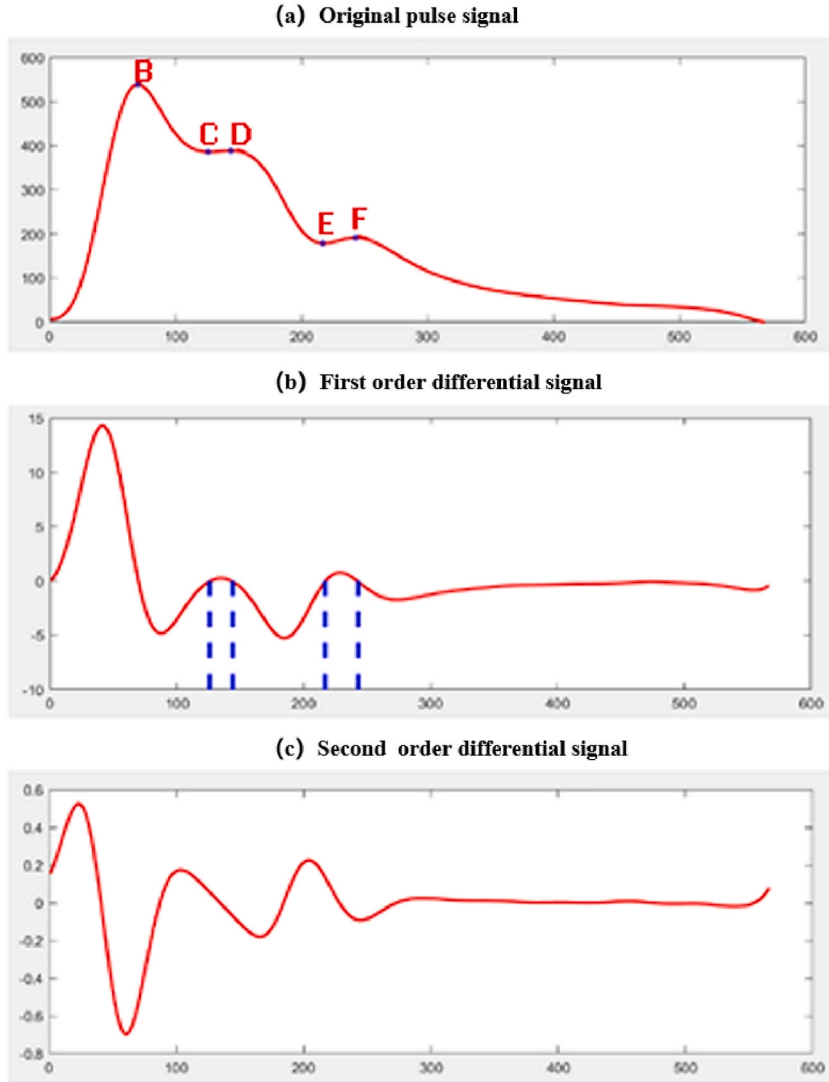


Fig. 11. Time domain feature extraction of Type III pulse waveform.

$$\text{Precision} = \frac{\text{TP}}{\text{TP} + \text{FN}} \quad (2)$$

Recall, also known as sensitivity or true positive rate, is a vital metric that assesses the proportion of correctly predicted positive instances relative to all actual positive instances. We calculated recall according to [formula \(3\)](#):

$$\text{Recall} = \frac{\text{TP}}{\text{TP} + \text{FP}} \quad (3)$$

The F1-score is a comprehensive metric that combines precision and recall into a single measure, providing a balanced assessment of the model's performance. It takes into account both the Precision, which measures the accuracy of positive predictions, and the Recall, which measures the ability to capture positive instances. F1-score was computed using [formula \(4\)](#):

$$\text{F1 - score} = \frac{2 \times \text{Precision} \times \text{Recall}}{\text{Precision} + \text{Recall}} \quad (4)$$

3. Results

3.1. Comparison of participant demographics

The demographic information of 133 patients with different degrees of coronary artery occlusion was shown in [Table 4](#). The

Table 2
Time domain features of the pulse signal.

Feature type	Feature parameter	Feature name
Magnitude	h1	Main wave amplitude
	h2	Main wave gorge amplitude
	h3	Wave front dicrotic amplitude
	h4	Dicrotic notch amplitude
	h5	Dicrotic wave amplitude
Time	w1	the width of main wave in its 1/3 height position
	w2	he width of main wave in its 1/5 height position
	t1	Main wave phase
	t2	Main wave gorge phase
	t3	Wave front dicrotic phase
Proportion	t4	Dicrotic notch phase
	t5	Dicrotic wave phase
	T	Pulse cycle
	h2/h1	Main wave gorge main Wave amplitude ratio
	h3/h1	Wave front dicrotic amplitude Main wave amplitude
	h4/h1	Dicrotic notch main wave amplitude ratio
	h5/h1	Dicrotic wave main wave amplitude ratio
	t1/T	Time ratio
	t1/t4	Time ratio
	t5/t4	Time ratio
w1/T	Pulse width cycle ratio	
w2/T	Pulse width cycle ratio	

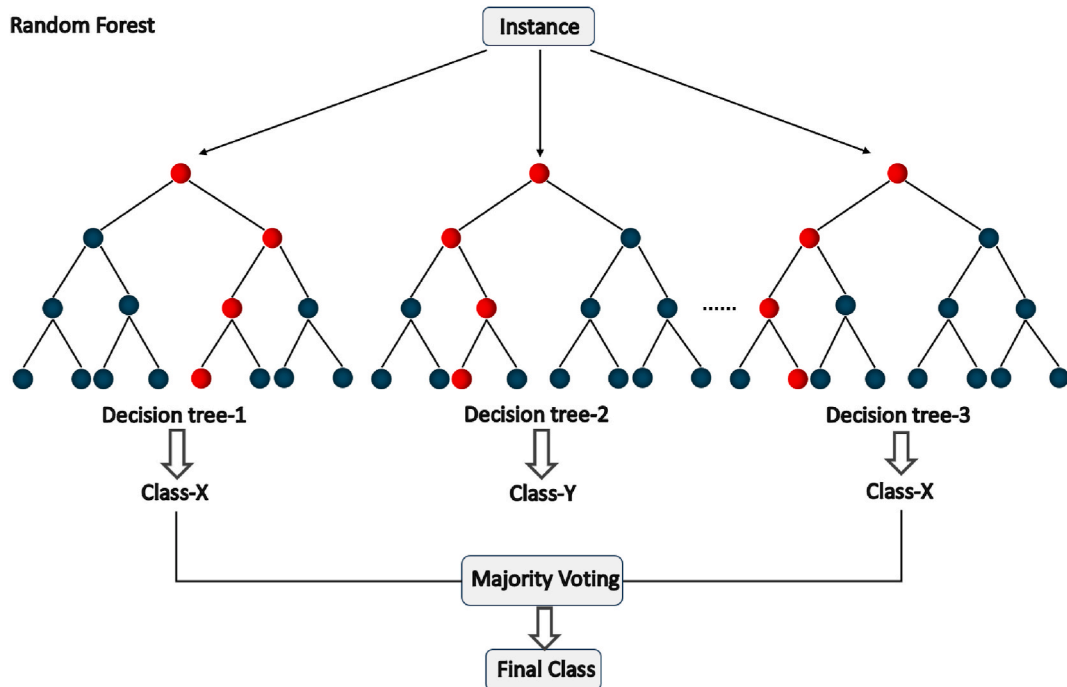


Fig. 12. Classification process based on the RF algorithm.

Table 3
Confusion matrix.

	Predicted Positive	Predicted Negative
Actual Positive	TP	FP
Actual Negative	FN	TN

Table 4

A comparison of demographical information among groups with different degrees of coronary artery occlusion.

Group	N	Gender		Age($\bar{x} \pm s$)
		Male	Female	
Group1	66	29	37	66.181 \pm 9.062
Group2	27	11	16	68.592 \pm 8.266
Group3	40	22	18	66.000 \pm 8.846
χ^2/F	–	1.694		0.851
P	–	0.429		0.429

analysis revealed no statistically significant differences in gender composition and age among different groups ($P > 0.05$). This indicates that the distribution of gender and age was similar across the participant groups, ensuring a balanced representation of participants in this study.

3.2. Comparison of wrist pulse and FPPG features

The time-domain features of the wrist pulse and FPPG signals were compared among the three groups and presented in this section. The analysis aims to reveal the differences and similarities in these features among the different degrees of coronary artery occlusion.

The Kruskal-Wallis test results for patients with different degrees of coronary artery occlusion are shown in Table 5. Specifically, t4 and T values were found to be significantly lower in Group 2 compared to Group 1 ($P < 0.05$). No statistically significant differences were found in other parameters. In this context, t4 represents the systolic time value of the heart, while T represents the cardiac cycle. Notably, the T demonstrated a consistent downward trend from the Group1 to Group2 and further to Group 3. These findings suggest potential associations between the degree of coronary artery occlusion and changes in t4 and T values.

3.3. Development and evaluation of models for assessing the severity of coronary artery occlusion

In this study, RF algorithms were employed to establish three distinct models for assessing the severity of coronary artery occlusion. Model 1 was based on the time-domain features of wrist pulse, Model 2 utilized time-domain features of FPPG, and Model 3 combined time-domain features of both wrist pulse and FPPG, along with PWTT. The assessment and comparison of the performance of these models were conducted using confusion matrices, Accuracy, Precision, Recall, and F1-score.

The confusion matrices of the different models were presented as the ratio of correctly predicted positive samples to all positive sample predictions, facilitating visual comparison. Figs. 13–15 depicted the confusion matrices for the classification results of Model 1, Model 2, and Model 3, respectively. Additionally, Tables 6–8 provided the four-evaluation metrics for each model. Table 9 showcased comparisons of Accuracy, Precision, Recall, and F1-score for the three models, providing a comprehensive overview of the performance measures for each model. Analysis of these figures and tables indicates that Model 3 exhibits superior performance.

4. Discussion

CHD is closely associated with endothelial damage in the coronary arteries, which can be caused by various factors including high blood pressure, hyperlipidemia, smoking, diabetes, and inflammation. The accumulation of lipid plaques in the damaged arteries can lead to partial or complete vascular blockage, resulting in alterations in hemodynamic parameters. These alterations are directly reflected in the pulse wave. Therefore, analyzing changes in the pulse wave's features, such as shape, intensity, speed, and rhythm, can detect variations in the function and state of human arteries.

In this research, we simultaneously acquired radial pressure pulse waves and FPPG. Time-domain features were extracted respectively, and based on these, the PWTT was calculated. This methodology enables the acquisition of multi-dimensional cardiovascular data, providing a breadth and depth of information that surpasses conventional single-source signal collection methods. The comparison among different groups revealed that the values of "t4" and "T" were lower in Group 2 (50% \leq stenosis in a major coronary vessel<70%) compared to Group 1 (stenosis in a major coronary vessel<50%). This indicates a shortened left ventricular systolic period, a shortened pulse cycle, and an increased heart rate in Group 2 and Group3. These phenomena may potentially be due to compensatory mechanisms of cardiac blood supply in response to coronary artery occlusion: In the event of arterial lumen damage, the

Table 5

A comparison of wrist pulse features among groups with different degrees of coronary artery occlusion.

Group	N	t4	T
Group1	66	0.350 (0.322,0.365)	0.903 (0.826, 1.022)
Group2	27	0.339 (0.309,0.354) \blacktriangle	0.860 (0.771,0.902) \blacktriangle
Group3	40	0.339 (0.318,0.359)	0.855 (0.782, 0.985)
H		6.698	7.789
P	–	0.035	0.020

Note: \blacktriangle , compared with Group 1, $P < 0.05$.

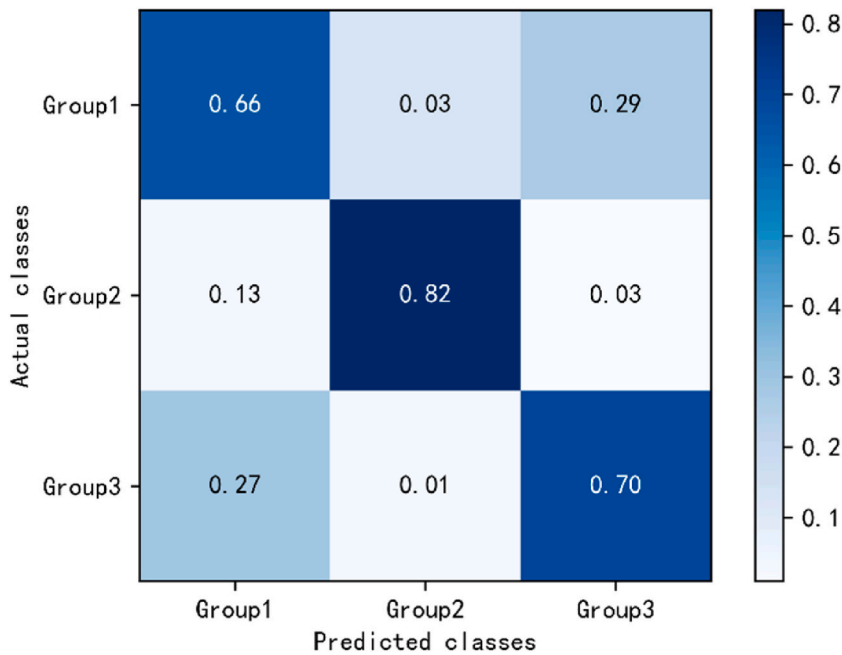


Fig. 13. Confusion matrices for Model 1.

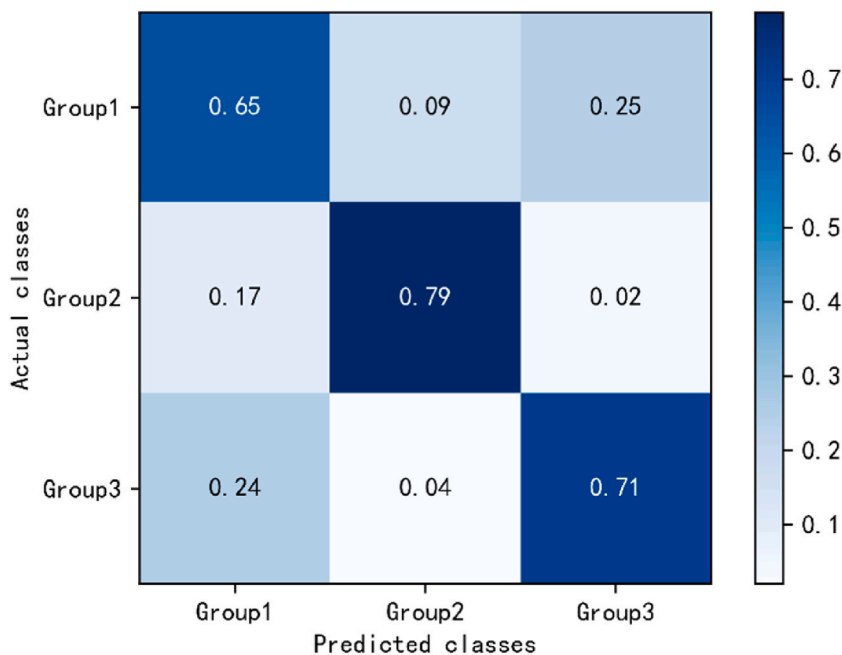


Fig. 14. Confusion matrices for Model 2.

heart may adapt by adjusting the duration of the cardiac cycle (T) to accommodate reduced blood flow, an adjustment that is critical for myocardial blood supply. This adaptation may manifest as an increase in heart rate, with the objective of maintaining a balance between myocardial oxygen demand and supply. The elevation in heart rate is key to maintaining adequate cardiac output and myocardial oxygenation, reflecting the cardiovascular system's ability to maintain a complex equilibrium during the progression of coronary artery disease.

Multi-source information fusion is a process of comprehensive processing and utilization of information from different sources, aimed at addressing complex pattern recognition or improving classification performance [20]. It can be divided into data-level fusion, feature-level fusion, and decision-level fusion [21]. In this study, we employed data-level fusion and feature-level fusion methods to

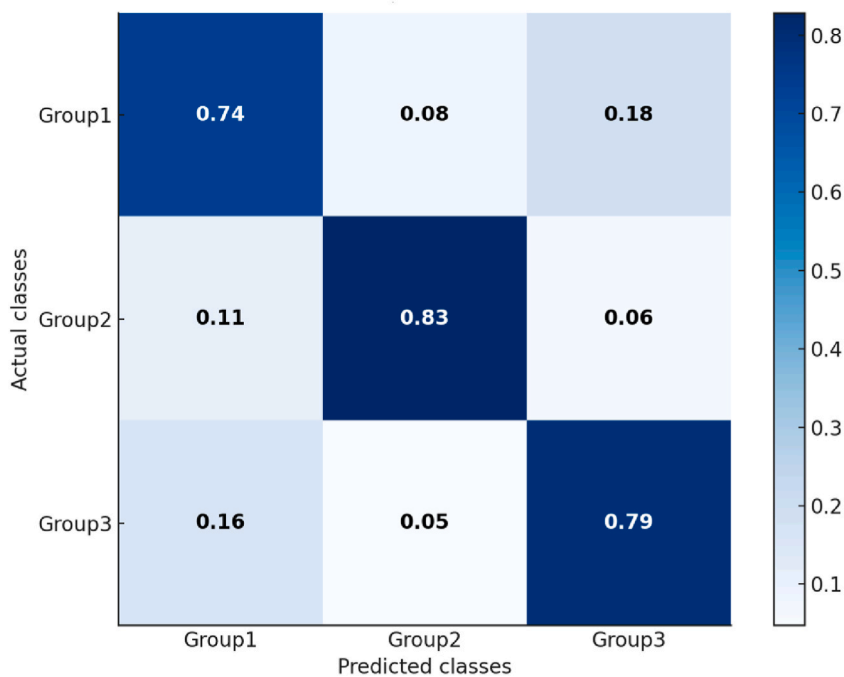


Fig. 15. Confusion matrices for Model 3.

Table 6

Evaluation metrics for the Model 1 (%).

Group	Group1(N = 66)	Group2(N = 27)	Group3(N = 40)
Precision	66.67	82.89	70.77
Recall	57.58	95.45	69.70
F1-score	61.79	88.73	70.23
Average Precision	73.44		
Average Recall	74.24		
Average F1-score	73.58		
Accuracy	74.24		

Table 7

Evaluation metrics for the Model 2 (%).

Group	Group1(N = 66)	Group2(N = 27)	Group3(N = 40)
Precision	65.45	79.45	71.43
Recall	54.55	87.88	75.76
F1-score	59.50	83.45	73.53
Average Precision	72.11		
Average Recall	72.73		
Average F1-score	72.16		
Accuracy	72.73		

Table 8

Evaluation metrics for the Model 3 (%).

	Group1(N = 66)	Group2(N = 27)	Group3(N = 40)
Precision	73.85	82.86	79.37
Recall	72.73	87.88	75.76
F1-score	73.28	85.29	77.52
Average Precision	78.69		
Average Recall	78.79		
Average F1-score	78.70		
Accuracy	78.79		

Table 9
Comparison of evaluation metrics of each model (%).

	Model 1	Model 2	Model 3
Average Precision	73.44	72.11	78.69
Average Recall	74.24	72.73	78.79
Average F1-score	73.58	72.16	78.70
Accuracy	74.24	72.73	78.79

process the collected multi-dimensional cardiovascular data. The research results show that Model 3, which incorporates both wrist pulse and FPPG features, surpassed Model 1 (solely utilizes wrist pulse features) and Model 2 (relies solely on FPPG features). Model 3 achieved an Accuracy, Precision, Recall, and F1-score of 78.79%, 78.69%, 78.79%, and 78.70%, respectively. Compared to Model 1, Model 3 exhibited a 4.55% higher Accuracy, 5.25% higher Precision, 4.55% higher Recall, and 5.12% higher F1-score. Similarly, it outperformed Model 2 with a 6.06% higher Accuracy, 6.58% higher Precision, 6.06% higher Recall, and 6.54% higher F1-score. The wrist pressure pulse wave has the capability to indicate arterial stiffness, hypertension, atherosclerosis, and other anomalies. Additionally, as blood traverses peripheral micro-arteries, capillaries, and micro-venules during circulation, it causes pulsatile changes in blood volume within these microvessels. These changes, as exemplified by FPPG, can reflect essential cardiovascular information, such as cardiac function, blood flow, peripheral vessels, and microcirculation. The synergy of pressure and photoelectric sensors enables cross-verification or mutual supplementation of the collected information, enhancing the reliability of the captured signals. This approach, by compensating for the limitations of individual sensors, acquires enough important information and thereby improves the reliability, robustness, and generalization ability of the identification model.

5. Conclusions

The fusion of wrist pulse features and FPPG features has demonstrated practical value in detecting the degree of coronary artery obstruction in CHD patients. It improves the accuracy of diagnosis and monitoring, making it applicable to research and development of wearable pulse diagnostic devices. Notably, this technology offers an effective and non-invasive approach in the early detection and management of the condition. To further advance the analysis and application of this method, future efforts should focus on utilizing larger datasets, incorporating additional types of pulse features, and exploring new AI technologies such as deep learning and ensemble learning.

Data availability statement

The data that has been used is confidential.

CRediT authorship contribution statement

M.A. Xiaotian: Writing – original draft, Visualization, Validation, Methodology, Investigation, Formal analysis, Data curation. **Rui Guo:** Writing – review & editing, Software, Resources, Project administration, Methodology, Investigation, Funding acquisition, Formal analysis, Data curation, Conceptualization. **Chunke Zhang:** Validation, Investigation, Data curation. **Jianjun Yan:** Visualization, Software, Resources, Project administration, Methodology, Formal analysis, Data curation. **Guangyao Zhu:** Visualization, Methodology, Formal analysis. **Wenjie Wu:** Investigation, Data curation. **Haixia Yan:** Supervision, Methodology. **Leixin Hong:** Formal analysis.

Declaration of competing interest

The authors declare that they have no known competing financial interests or personal relationships that could have appeared to influence the work reported in this paper.

References

- [1] P. Deloukas, S. Kanoni, C. Willenborg, M. Farrall, T.L. Assimes, J.R. Thompson, E. Ingelsson, D. Saleheen, J. Erdmann, the CARDIoGRAMplusC4D Consortium, Large-Scale association analysis identifies new risk loci for coronary artery disease, *Nat. Genet.* 45 (2012) 25–33, <https://doi.org/10.1038/ng.2480>. Epub 2012 Dec 2. PMID: 23202125; PMCID: PMC3679547. Author 1, A.; Author 2, B. Title of the chapter. In Book Title, 2nd ed.; Editor 1, A., Editor 2, B., Eds.; Publisher: Publisher Location, Country, 2007; Volume 3, pp. 154–196.
- [2] C.W. Tsao, A.W. Aday, Z.I. Almarzoq, A. Alonso, A.Z. Beaton, M.S. Bittencourt, A.K. Boehme, A.E. Buxton, A.P. Carson, Y. Commodore-Mensah, M.S.V. Elkind, K.R. Evenson, C. Eze-Nliam, J.F. Ferguson, G. Generoso, J.E. Ho, R. Kalani, S.S. Khan, B.M. Kissela, K.L. Knutson, D.A. Levine, T.T. Lewis, J. Liu, M.S. Loop, J. Ma, M.E. Mussolino, S.D. Navaneethan, A.M. Perak, R. Poudel, M. Rezk-Hanna, G.A. Roth, E.B. Schroeder, S.H. Shah, E.L. Thacker, L.B. VanWagner, S. Virani, J.H. Voeks, N.Y. Wang, K. Yaffe, S.S. Martin, Heart disease and stroke statistics-2022 update: a report from the American heart association, *Circulation* 145 (2022) 528, <https://doi.org/10.1161/CIR.000000000001052>. Epub 2022 Jan 26. Erratum in: *Circulation*. 2022 Sep 6;146(10):e141. PMID: 35078371.
- [3] Report on cardiovascular health and diseases in China 2021:an updated summary, *J. Cardiovasc. Pulm. Dis.* 41 (2022) 1205–1211.
- [4] K. Thygesen, J.S. Alpert, H.D. White, Joint ESC/ACCF/AHA/WHF task force for the redefinition of myocardial infarction. Universal definition of myocardial infarction, *J. Am. Coll. Cardiol.* 50 (2007) 2173–2195, <https://doi.org/10.1016/j.jacc.2007.09.011>. PMID: 18036459.

- [5] A.V. Poznyak, D. Bharadwaj, G. Prasad, A.V. Grechko, M.A. Sazonova, A.N. Orekhov, Renin-angiotensin system in pathogenesis of atherosclerosis and treatment of CVD, *Int. J. Mol. Sci.* 22 (2021) 6702, <https://doi.org/10.3390/ijms22136702>. PMID: 34206708; PMCID: PMC8269397.
- [6] J. Chen, P. Aronowitz, Congestive heart failure, *Med. Clin.* 106 (2022) 447–458, <https://doi.org/10.1016/j.mcna.2021.12.002>. Epub 2022 Apr 4. PMID: 35491065.
- [7] K.M. Abdelrahman, M.Y. Chen, A.K. Dey, R. Virmani, A.V. Finn, R.Y. Khamis, A.D. Choi, J.K. Min, M.C. Williams, A.J. Buckler, C.A. Taylor, C. Rogers, H. Samady, C. Antoniadis, L.J. Shaw, M.J. Budoff, U. Hoffmann, R. Blankstein, J. Narula, N.N. Mehta, Coronary computed tomography angiography: from clinical uses to emerging technologies: JACC state-of-the-art review, *J. Am. Coll. Cardiol.* 76 (2020) 1226–1243, <https://doi.org/10.1016/j.jacc.2020.06.076>. PMID: 32883417; PMCID: PMC7480405.
- [8] C. Peng, H. Wu, S. Kim, X. Dai, X. Jiang, Recent advances in transducers for intravascular ultrasound (IVUS) imaging, *Sensors* 21 (2021) 3540, <https://doi.org/10.3390/s211103540>. PMID: 34069613; PMCID: PMC8160965.
- [9] U.J. Schoepf, P.L. Zwerner, G. Savino, C. Herzog, J.M. Kerl, P. Costello, Coronary CT angiography, *Radiology* 244 (2007) 48–63, <https://doi.org/10.1148/radiol.2441052145>. Epub 2007 May 10. PMID: 17495176.
- [10] Z.C. Lu, S. Zhang, Y.M. Yang, *Engineering analysis for pulse wave and its application in clinical practice 8–11*, Science Press, 2006, pp. 139–140.
- [11] S. Kumar, K. Veer, S. Kumar, Development of an adjustable pulse measurement system for determining the precise position for recording high wrist pulse signals, *MAPAN* 38 (2023) 689–706, <https://doi.org/10.1007/s12647-023-00671-9>.
- [12] A.S. Al Fahoum, A.O. Abu Al-Haija, H.A. Alshraideh, Identification of coronary artery diseases using photoplethysmography signals and practical feature selection process, *Bioengineering* 10 (2) (2023) 249.
- [13] C. Guo, Z. Jiang, H. He, Y. Liao, D. Zhang, Wrist pulse signal acquisition and analysis for disease diagnosis: a review, *Comput. Biol. Med.* (2022) 143, <https://doi.org/10.1016/j.combiomed.2022.105312>. Epub ahead of print. PMID: 35203039.
- [14] J. Yan, X. Cai, G. Zhu, R. Guo, H. Yan, Y. Wang, A non-invasive blood pressure prediction method based on pulse wave feature fusion, *BIOMED SIGNAL PROCES* 74 (2022), <https://doi.org/10.1016/j.bspc.2022.103523>.
- [15] L.A. Fleisher, J.A. Beckman, K.A. Brown, H. Calkins, E.L. Chaikof, K.E. Fleischmann, et al., ACC/AHA 2007 guidelines on perioperative cardiovascular evaluation and care for noncardiac surgery: a report of the American College of Cardiology/American heart association task force on practice guidelines (writing committee to revise the 2002 guidelines on perioperative cardiovascular evaluation for noncardiac surgery) developed in collaboration with the American society of echocardiography, American society of nuclear Cardiology, heart rhythm society, society of cardiovascular anesthesiologists, society for cardiovascular angiography and interventions, society for vascular medicine and biology, and society for vascular surgery, *J. Am. Coll. Cardiol.* 50 (2007) e159–e241, <https://doi.org/10.1016/j.jacc.2007.09.003>.
- [16] S. Kumar, S. Kumar, K. Veer, Pulse (nadi) analysis for disease diagnosis: a detailed review, *Proc. Natl. Acad. Sci., India, Sect. A Phys. Sci.* 93 (2023) 135–145, <https://doi.org/10.1007/s40010-022-00800-0>.
- [17] J. Hou, Y. Zhang, S. Zhang, et al., A novel angle extremum maximum method for recognition of pulse wave feature points, *Comput. Methods Progr. Biomed.* 189 (2020) 105321.
- [18] J. Yan, X. Cai, S. Chen, R. Guo, H. Yan, Y. Wang, Ensemble learning-based pulse signal recognition: classification model development study, *JMIR Med Inform* 9 (2021) e28039, <https://doi.org/10.2196/28039>. PMID: 34673537.
- [19] L. Breiman, Random forests, *Mach. Learn.* 45 (2001) 5–32, <https://doi.org/10.1023/A:1010933404324>.
- [20] C. Guo, Q. Song, Y. Liu, Research on the application of multi-source information fusion in multiple gait pattern transition recognition, *Sensors* 22 (21) (2022 Nov 6) 8551, <https://doi.org/10.3390/s22218551>. PMID: 36366248; PMCID: PMC9658818.
- [21] Q. Sen, Z. Hongkai, J. Nan, et al., Giancarlo Fortino, Multi-sensor information fusion based on machine learning for real applications in human activity recognition: state-of-the-art and research challenges, *Inf. Fusion* 80 (2022) 241–265, <https://doi.org/10.1016/j.inffus.2021.11.006>.